Processability Assessment of Recycled Polymeric Nonwoven Materials in Injection Molding, Film Extrusion and Additive Manufacturing

Polymer Engineering & Science

WILEY | spe INSPIRING PLASTICS PROFESSIONALS

RESEARCH ARTICLE OPEN ACCESS

Processability Assessment of Recycled Polymeric Nonwoven Materials in Injection Molding, Film Extrusion and Additive Manufacturing

Daniele Battegazzore[1] | Fulvia Cravero[1] | Giulia Bernagozzi[1] | Rossella Arrigo[1,2] | Alberto Frache[1,2]

[1]Dipartimento di Scienza Applicata e Tecnologia Politecnico di Torino, Alessandria Site, Alessandria, Italy | [2]Local unit of National Interuniversity Consortium of Materials Science and Technology (INSTM), Florence, Italy

Correspondence: Daniele Battegazzore (daniele.battegazzore@polito.it)

Received: 21 March 2026 | **Revised:** 15 April 2026 | **Accepted:** 16 April 2026

Keywords: 3D printing | FFP2 masks | film extrusion | injection molding | recycled polypropylene | rheology

ABSTRACT

Nonwoven waste from new or postuse surgical and FFP2 face masks represents a complex multimaterial stream with significant upcycling potential. Material characterization identified PP and PE as the predominant components, with minor fractions of PET, cellulose fibers, and inorganic fillers. Rheology was used to classify different waste streams: postuse surgical masks exhibited low viscosity and negligible yield stress, making it suitable for injection molding; postuse FFP2 masks showed higher zero-shear viscosity, pronounced shear-thinning, and significant yield stress, ensuring filament stability and shape retention in material extrusion additive manufacturing; new surgical masks displayed intermediate viscosity and shear-thinning, enabling smooth and anisotropic film production via extrusion. Blending strategies of postuse masks enabled tuning of rheological and mechanical properties: injection-molded samples maintained homogeneous mechanical performances within ~20% deviation, while 3D-printed blends exhibited surface roundness and roughness associated with postuse FFP2 content. Overall, mask-derived nonwovens can be successfully upcycled into sustainable feedstock.

1 | Introduction

Recent global market analyses indicate that polymeric nonwoven materials represent a considerable and growing segment of engineered materials used across hygiene, medical, filtration, automotive, and construction industries. In 2024, global consumption of nonwoven fabrics reached approximately 19 million tons, showing modest fluctuations after peaking near 20 million tons in 2021, and reflecting a long-term average annual growth rate of around 3.4% over the past decade. The global market value in 2024 was estimated at roughly 66.5 billion USD, and projections suggest an expansion to about 23 million tons by 2035 [1].

This production and consumption volume reflects the importance of nonwoven materials: they are engineered directly from fibers into sheet or web forms without traditional weaving, imparting tailored structural and functional properties for specific applications. As an example, hygiene products like wipes and diapers account for a substantial share of the nonwoven market, while technical applications such as filtration and automotive components further reinforce demand.

To contextualize these figures relative to other major material streams, it is useful to compare nonwoven volumes with global packaging materials and waste. While precise global production figures for all packaging materials vary by data source and material type, packaging remains one of the largest single contributors to material use and waste. In 2019, global plastic waste generation reached approximately 353 million metric tons, with packaging responsible for around 40% of that total [2, 3].

Highlights

- Postuse masks upcycled into processable polymer materials.
- Recycled material is suitable for injection molding processes.
- Recycled material is ideal for three-dimensional printing.
- Recycled material enabled smooth film extrusion.
- Blending materials tuned rheology while preserving mechanics.

This implies that plastic packaging alone contributed on the order of 140 million tons of plastic waste globally, far exceeding the total annual nonwoven production volume.

This comparison underscores two key points for sustainable end-of-life strategies. Firstly, although nonwoven materials represent a significant engineered material stream with specialized applications, material volumes destined for packaging and associated waste streams remain several times larger. On the other hand, current recycling systems are stressed by large volumes of complex material waste, highlighting the need for improved recycling and higher-value valorization approaches, such as upcycling for complex multi-polymer materials like nonwoven blends [2, 4].

Against this broader background of growing nonwoven production and increasing pressure on waste management systems, the COVID-19 pandemic represented an unprecedented stress test for polymer-based disposable products. Starting in 2020, the SARS-CoV-2 outbreak profoundly altered daily habits and public behavior, leading to the widespread adoption of personal protective equipment (PPE), surface sanitization practices, and social distancing measures as primary tools to limit virus transmission. Most PPE, including face masks and respirators, are manufactured from polymeric nonwoven materials and are designed for single or short-term use, resulting in large and sudden waste streams [5–7].

Currently, available PPE can be broadly classified into surgical masks and respirators. Surgical masks are mainly used in healthcare settings to reduce contamination risks for patients, while respirators are designed to protect users from inhaling harmful particles and are classified according to European standards as FFP1, FFP2, and FFP3 [8]. Beyond their limited duration of use, these devices also have a defined shelf life—typically between 3 and 5 years—due to regulatory requirements for medical and sanitary products. Consequently, both postuse PPE and unused or expired stockpiles contribute significantly to polymeric waste generation.

This issue is exemplified by recent disposal cases: in Italy alone, approximately 218 million face masks (corresponding to about 2500 tons) were destroyed at a cost of around 700,000 euros, despite the fact that similar polymeric materials may have a positive market value when recycled [9]. These figures highlight the urgent need for sustainable end-of-life scenarios not only for used PPE but also for production offcuts, out-of-spec items, and expired products.

Although the World Health Organization declared the end of the COVID-19 global health emergency in May 2023, PPE consumption is not expected to return to prepandemic levels [10]. Market analyses indicate that sustained awareness of infection prevention has led to structurally higher demand for disposable masks, with the US surgical mask market alone estimated at approximately 73 million USD in 2023—about 25% higher than in 2019 [6]. This trend is further supported by epidemiological evidence showing a marked reduction in seasonal influenza cases during periods of widespread mask usage. As a result, PPE waste management remains a long-term challenge rather than a temporary consequence of the pandemic.

From a materials perspective, face masks and respirators represent a particularly complex nonwoven waste stream. Their heterogeneity includes polymeric fibrous layers, elastic ear loops, and metallic nose wires, which complicate separation and conventional recycling operations [11]. Surgical masks typically consist of three polypropylene nonwoven layers, including a central meltblown filter layer and hydrophobic outer layers. Respirators such as FFP2 and FFP3 devices generally contain five or more layers made of different polymers, including polypropylene (PP), polyethylene (PE), and polyethylene terephthalate (PET). Natural polymers, such as cellulose-based fibers, may also be present in specific filter designs [8, 12–15].

The presence of multilayer and multimaterial architectures strongly limits the efficiency of traditional recycling routes, which often result in material downcycling. This challenge is particularly relevant when mixed polymer streams are processed together, a scenario that is increasingly common in industrial waste management and represents one of the main barriers to achieving low-waste or circular material systems [16, 17]. Nevertheless, production scraps and preconsumer wastes offer advantages in terms of traceability and material consistency, reducing the need for complex sorting operations.

Within this context, this paper presents a case study focused on the upcycling potential of polymeric nonwoven blends derived from surgical masks and FFP2 respirators. While several recycling strategies for disposable masks have been reported in the literature—including mechanical recycling, carbonization processes, incorporation into construction materials, and blending with virgin polymers—these approaches generally rely on downcycling or on the addition of external fillers and matrices [13, 18–23]. By contrast, upcycling requires that waste materials be transformed into products with enhanced value, performance, or functionality, rather than being reintroduced into their original application.

Assuming a dedicated and separate collection from conventional mixed polyolefin streams, both postuse and unused surgical masks and respirators were considered in this study. After preliminary material characterization, the suitability of the recovered materials for different industrial processing technologies—including injection molding, casting, and material extrusion additive manufacturing (MEAM)—was assessed.

Particular attention was paid to the rheological behavior of the recycled materials, as process feasibility is strongly dependent on viscosity and flow characteristics within the shear rate ranges specific to each technology [24–27]. The ultimate objective is to identify transformation routes that enable true upcycling of polymeric nonwoven PPE waste, extending its application potential beyond its original single-use function.

Importantly, the findings of this study are not limited to face masks. The approach of combining thorough material characterization, targeted collection, and evaluation of multiple processing technologies can be extended to a wide range of polymeric nonwoven products, including wipes, filtration media, hygiene items, and technical fabrics. The key insight is that concentrated collection of a specific product type, as successfully implemented for masks during the pandemic, ensures higher material consistency, lower contamination, and better traceability. These factors make industrial upcycling significantly easier and more effective, as the properties of the input material are well known and predictable. Applying this strategy to other nonwoven sectors could enable similar high-value transformation, promoting circular economy practices and extending the life and utility of polymeric nonwoven materials well beyond their original applications.

2 | Materials and Methods

2.1 | Materials

The after use surgical and FFP2 masks were collected by volunteers in schools and brought to Greenlife multiservices s.r.l. for the sanitization with ozone generators Ozonplus [23] (Figure 1 Phase 1).

For both kinds of masks, the facial filtering parts were coded respectively as M1 and M2 after manual separation of metal nose clips and ear loops (Figure 1 Phase 2).

New surgical masks produced for the Italian government and delivered to schools and public buildings coded as M3 are used after manual separation of metal nose clips (Figure 1 Phase 2).

2.2 | Equipment and Process of Recycling

All kinds of masks were hot pressed at 190°C with Collin P 200 T machine (Figure 1 Phase 3) and then grinded (diameter smaller than 5 mm) with a Piovan Rsp15/15 mill (Figure 1 Phase 4). The obtained cM1, cM2 and cM3 granules were processed and mixed in several percentages by means of a manually fed mini-extruder (Xplore MC 15) coded as "small scale" in Figure 2. The screw speed was maintained at 50 rpm during feeding time and increased to 100 rpm for the 3 min residence time. The processing temperature was selected at 190°C. The materials obtained are referred to as rM1, rM2, and rM3, and all their blends are indicated by such abbreviation and a number identifying the corresponding relative weight percentage.

Selected materials were processed with a ThermoFisher Scientific twin-screw extruder Process 11 (coded as "large scale" in Figure 2). After the die exit, the extrudate was cooled in a water-containing tank and pelletized with a rotating cutter Varicut pelletizer 11 mm. The screw speed varied from 50 to 150 rpm. The heating temperature profile was set from 180°C (hopper) to 200°C (die). The screw profile adopted during all extrusions was already reported in the literature [23]. A volumetric feeder (MT model from Brabender) was used to supply the mix located at the beginning of the extruder with an extrusion output of 0.1 kg/h.

FIGURE 1 | Mechanical recycling phases of after use surgical masks (M1), FFP2 masks (M2), and new surgical masks (M3).

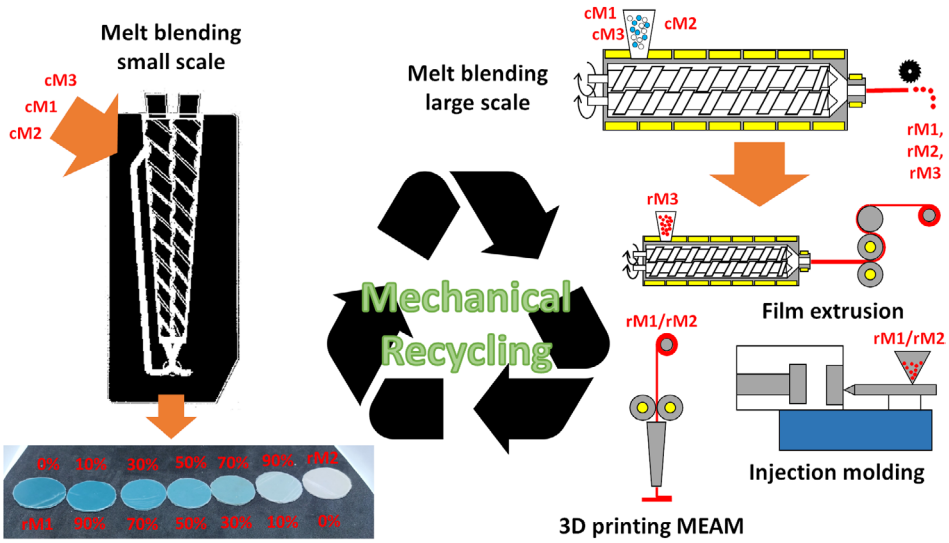

FIGURE 2 | Mechanical recycling phases: small and large scale melt blending.

Pellets obtained by extrusion were processed using an injection molding machine Babyplast 6/10P at 180°C, with mold temperature of 40°C, cooling time of 15.5 s, packing pressure of 70 bar for 8.5 s. Ten 5A type specimens according to the standard ISO527 were prepared and used for tensile tests.

The film extrusion was performed using a co-rotating twin screw extruder LEISTRITZ ZSE 18/40 D. The screw speed was fixed at 150 rpm. The heating temperature was set in the eight heated barrel blocks from 180°C to 190°C. A gravimetric feeder was used in the main hopper with a throughput of 0.5 kg/h. The used screw profile is reported in Supporting Information (Figure S1). A special equipment made of a flat die (40 × 1 mm hole, Figure S1) and two calenders (Eurotech Extrusion Machinery S.r.l.) were used to press and stretch the molten polymers in the machine direction. The two calenders are not heated. The distance between them and the applied pressure on the film are manually regulated by moving down the upper calender.

Felfil Evo filament making machine (Figure S2) has been used to produce a filament with a nominal diameter of 1.75 mm in order to feed MEAM instrument. The Felfil Evo filament making machine is made of a single-screw extruder, a series of horizontally cooling fans and then a spooler to collect the filament. Before collecting the filament, it passes through two counter-rotating rollers and through a laser sensor that checks the diameter in order to maintain it as constant as possible, by automatically adjusting the spooler speed. The main parameters that can be modified in order to obtain a filament of adequate quality (constant and circular diameter, low roughness) are: temperature, screw speed and fan speed. Each formulation requires a different combination of parameters that will be further discussed.

Roboze One 3D printer equipped with a 0.6 mm nozzle was used to make 3D printed objects with the help of Simplify 3D software. In order to verify the printing quality, a nut was designed with six faces 20 mm wide and a central hole with a diameter of 10 mm. The extruder temperature and the bed temperature of the 3D printer were set at 260°C and 50°C, respectively. The objects have an infill equal to 30%, and they were 3D printed with a printing speed set at 30 mm/s.

A summary table (Table 1) reports the material origin, processing history, and final application (e.g., extrusion, injection molding, film production, and MEAM), providing an immediate overview of how each material stream evolves from postuse masks to its final use.

2.3 | Characterization Techniques

Thermal properties were evaluated by differential scanning calorimetry (DSC) using as equipment a DSC Q20 by TA Instruments. The samples, weighing 8 ± 1 mg, were put into a chamber with nitrogen and heated from 20°C to 270°C at 10°C/min twice. The information achieved from DSC analysis are crystallization temperature (T_c), assumed as the abscissa of the heat flow main peak during the cooling cycle, and crystallization enthalpy (ΔH_c), evaluated as the integral of the same peak.

Rheological analyses were carried out using a strain-controlled parallel plate geometry rheometer ARES (plate diameter: 25 mm), provided by TA Instrument. The analyses were made on compression molded samples (25 mm diameter and 1 mm thickness) obtained using a Collin P200T press at 190°C for 3 min.

In order to fit the experimental complex viscosity curves, a modified Carreau equation was used:

$$\eta^*(\omega) = \frac{\eta_0}{[1+(\lambda\omega)]^{(1-n)}} + \frac{\sigma_0}{\omega} \quad (1)$$

where σ_0 is the melt yield stress, η_0 is the zero-shear viscosity, λ is the relaxation time, and n is the dimensionless power law index.

Rheological characterization was also performed in non-isothermal elongational flow by using a RheoSpin apparatus

TABLE 1 | Summary table of sample codes, material origin, processing history, and final application.

Sample code	Origin of material	Processing history	Final application/ testing
M1, M2, M3	Different mask types	Hot pressing (190°C)	Intermediate materials coded cM1,cM2,cM3
rM1, rM2, rM3	Reprocessed mask granules (cM1, cM2, cM3)	Small-scale extrusion (190°C, Xplore MC 15)	rM1/rM2/rM3 neat and blends for characterizations
rM1, rM2, rM3	Reprocessed mask granules (cM1, cM2, cM3)	Large-scale twin-screw extrusion (180°C–200°C, Process 11)	rM1/rM2/rM3 neat and blends for application
Injection molded samples (rM1_rM2)	Extruded pellets/blends for application	Injection molding (180°C, Babyplast 6/10P)	Mechanical characterization
Extruded films (rM3)	Extruded pellets for application	Film extrusion (180°C–190°C, Leistritz ZSE 18/40 D)	Film characterization
Filaments (rM1_rM2)	Extruded pellets/blends for application	Filament extrusion (Felfil Evo)	MEAM feedstock
MEAM process 3D printed parts (rM1_rM2)	MEAM Filaments	MEAM (260°C nozzle, Roboze One)	Printability evaluation

(Figure S3). At the breaking of the filament, the current force and speed are registered.

Tensile tests were performed at room temperature with an Instron 5966 machine equipped with 2 kN pneumatic grips and a loading cell of 2 kN (error < 0.25%). The measurement parameters for testing dog-bone shaped samples were an initial strain rate of 1 mm/min that increased up to 10 mm/min once a deformation of 0.25% was exceeded. The tests on films were performed instead with a strain rate of 50 mm/min. The average values and corresponding standard deviations of the tensile modulus (E), elongation at break (ε), and maximum tensile strength (σ) were calculated and reported.

The surfaces' morphology was investigated using an EVO 15 scanning electron microscope (SEM) from Zeiss (beam voltage: 20 kV working distance: 8.5 mm). The filament surfaces were directly investigated by cutting small pieces while the sections were obtained by a brittle fracture in liquid nitrogen. All surfaces were covered with a sputtered gold layer before observation.

3 | Results and Discussion

3.1 | Masks Characterization

Surgical masks are generally characterized by three protective layers made of PP from different production technologies. On the other hand, the ear loop bands can be made of different materials [11, 14, 15, 28]. The ear loop parts have been removed in the collection of postuse masks (M1) while they have been kept in the new masks of certified origin (M3). A FTIR-ATR characterization of this second type of mask is reported in the Supporting Information to identify the material of the facial and ear loops (Figure S4).

FFP2 masks were also considered and sorted visually by type after collection and sanitization. Eighteen types of masks have been identified and statistically reported in the Supporting Information (Figure S5). The most numerous masks collected have PP and PE as constituent materials (see Supporting Information mask type "E" Figure S6). However, a smaller quantity of masks have one layer made of PET or cellulose (see supporting information mask type "S" and "B" Figures S7 and S8), in agreement with the literature [13].

All the FFP2 mask types have been processed as described in the materials and methods section at 180°C. It should therefore be noted that the presence of infusions (PET and cellulose fibers) is expected (also visible in DSC plot in Figure S9), and their effect on the material properties will be investigated in the next section.

3.2 | rM1, rM2, and rM3 Recycled Materials Characterization

The materials rM1, rM2, and rM3 obtained from three types of recycling based on surgical and FFP2 masks were characterized from a morphological and rheological point of view.

Figure 3 reports the SEM micrographs and corresponding EDX analyses of materials rM1, rM2, and rM3. rM1 exhibits a continuous PP matrix with embedded inorganic particles; the EDX analysis performed on the selected area S1 confirms the presence of calcium carbonate ($CaCO_3$), in agreement with literature data [11].

The fracture surface of rM2 shows filament-like structures protruding from the matrix. SEM observations highlight a fibrous morphology, while EDX analyses carried out on selected areas S2 and S3 mainly detect carbon and oxygen, indicating a polymeric

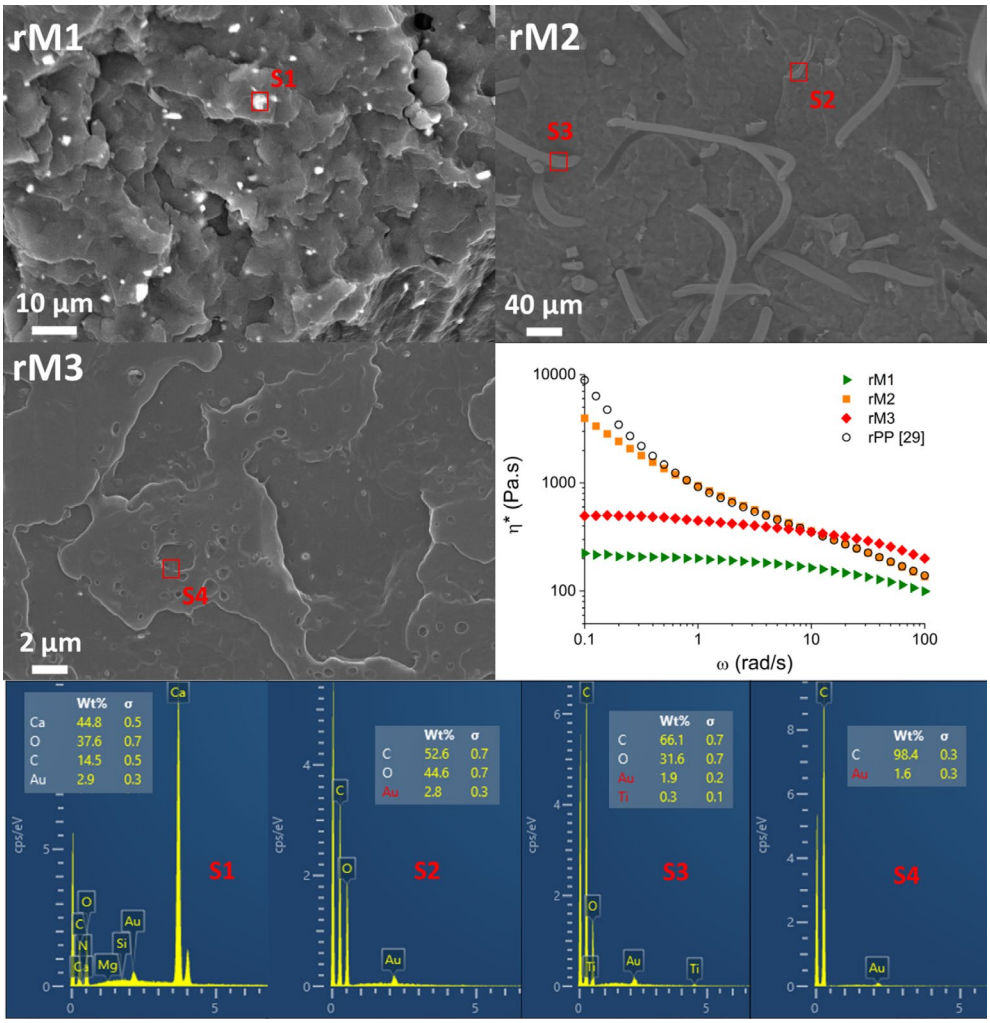

FIGURE 3 | SEM and EDX of the materials recycled from masks coded rM1, rM2, and rM3; Complex viscosity curves collected at 180°C for all recycled materials and a reference recycled rPP [29].

nature of the filaments. Traces of titanium are also observed, likely attributable to titanium dioxide (TiO_2), commonly used as a white pigment in polymeric fibers.

In contrast, rM3 displays a nearly smooth and rectilinear fracture surface with limited morphological variations. The EDX analysis performed on area S4 reveals only the presence of carbon, suggesting a homogeneous polymeric composition without detectable inorganic fillers.

In addition, Figure 3 includes the complex viscosity curves obtained through oscillatory measurements. The rheological response highlights differences among the investigated materials, reflecting their distinct microstructural features. In particular, the variations in the complex viscosity values and trends as a function of frequency can be correlated with the presence of inorganic fillers in rM1, fibrous polymeric structures in rM2, and the more homogeneous polymeric nature of rM3, as already evidenced by the SEM–EDX analysis.

The rheological curves in Figure 3 reveal distinct behaviors for the three materials. rM1 exhibits the lowest viscosity across the entire frequency range, and a well-pronounced Newtonian behavior, indicating that the dispersed inorganic fillers are not able to interfere with the relaxation of the polymeric chains. rM2 shows a pronounced increase in viscosity over the whole investigated frequency range, consistent with the embedded filament-like structures observed by SEM, which act as a network restricting chain mobility and disturbing the macromolecular dynamics. The figure also shows a commercial rPP reported in the literature [29], which confirms the similarity in rheological behavior with rM2. In fact, the rPP material contained infused additives, which account for the observed behavior. rM3 presents a curve quite similar to rM1, but shifted upward in viscosity across all frequencies, in agreement with SEM–EDX observations that indicate a homogeneous polymeric composition without significant inorganic fillers or network-like structures.

These differences in the rheological behavior can be further quantified using a modified Carreau model (Equation 1), which fits the frequency-dependent viscosity data with characteristic parameters such as zero-shear viscosity (η_0), a relaxation time constant (λ), and the power-law index (n). Such modeling allows the estimation of key rheological quantities—for example, the transition behavior between Newtonian and shear-thinning regimes—providing a numerical basis to compare the degree of shear thinning and structural effects among rM1, rM2, and rM3.

As reported in Table 2, the lower power-law index n for rM2 ($n = 0.61$) indicates a more pronounced shear-thinning behavior, whereas the similar n values of rM1 and rM3 suggest comparable flow behavior despite their different viscosity levels. The relaxation time λ is significantly higher for rM2, further supporting the presence of a more structured system with slower relaxation dynamics. Additionally, it should be noticed that, while rM1 and rM3 exhibit an almost negligible yield stress ($\boldsymbol{\sigma_0}$), consistent with fully developed Newtonian behavior, rM2 shows a markedly higher value. This result can be attributed to the previously discussed influence of the fiber-like structures on polymer chain relaxation. The high R^2 values confirm the excellent agreement between experimental data and the modified Carreau model.

Rheological characterization under non-isothermal elongational flow was also performed. As reported in Table S1, rM3 exhibits a significantly higher melt deformability compared to rM1, indicating a greater ability of the molten polymer to withstand elongational deformation before filament breakage. This behavior suggests enhanced melt extensibility for rM3, consistent with its higher zero-shear viscosity and more homogeneous polymeric structure observed in SEM–EDX analysis. Conversely, the lower deformability measured for rM1 reflects a reduced elongational stability of the melt, which can be associated with its lower viscosity and the presence of dispersed inorganic particles, known to promote stress concentration and earlier filament rupture under extensional flow. These results are in agreement with the literature, confirming that polymer systems with higher melt viscosity and fewer structural heterogeneities generally exhibit improved processability upon nonisothermal elongational flow [30].

The selection of specific processing routes based on rheological behavior is well supported by polymer processing literature. Rheological characteristics such as zero-shear viscosity (η_0), shear-thinning behavior, and yield stress (σ_0) are critical in determining a material's suitability for different manufacturing techniques. Shear-thinning behavior reduces melt viscosity at high shear rates, facilitating flow during high-speed processes such as injection molding and extrusion and lowering processing pressures and energy consumption [31]. In extrusion-based additive manufacturing (3D printing), a sufficiently high η_0 and pronounced shear thinning promote smooth extrusion through a nozzle and support shape retention after deposition; the presence of yield stress can help avoid premature dripping and improve dimensional stability of printed structures [32].

These established rheological principles explain the process suitability of the investigated formulations. rM1, with the lowest η_0 and negligible σ_0, aligns with requirements for injection molding, where low melt viscosity enables easy mold filling under high shear conditions. rM2, exhibiting the highest η_0, a more pronounced shear-thinning response (lower n), and a significant yield stress (σ_0), suggests that it is ideal for material extrusion 3D printing, as elevated viscosity and yield stress support shape fidelity and resist deformation after deposition. For extrusion processes, a high value of η_0 combined with an accentuated shear-thinning behavior is generally required to ensure dimensional stability at low shear rates and processability at high shear rates. Among the investigated formulations, rM3 exhibits an η_0 compatible with extrusion requirements; furthermore, this sample presents high deformability under elongational flow, suggesting its suitability for cast-extrusion operations. Nevertheless, careful optimization of the processing conditions could be required due to the limited shear-thinning behavior of this material [26].

TABLE 2 | Modified Carreau model parameters used for fitting the rheological curves of rM1, rM2, and rM3.

Sample	η_0 [Pa×s]	λ [1/s]	n	σ_0 [Pa]	R^2
rM1	202	0.10	0.72	2	0.99
rM2	774	0.84	0.61	332	0.99
rM3	465	0.17	0.73	5	0.98

3.3 | Recycling/Upcycling Technology Application

3.3.1 | Injection Molding

Injection molding is one of the most widely exploited industrial techniques for processing thermoplastic polymers due to its high productivity, dimensional precision, and adaptability to complex geometries. In the context of recycled or upcycled polymer materials, injection molding also plays a crucial role in adding value to waste streams by enabling the transformation of mechanically recovered polymers into new components with tailored properties. During injection molding, the molten polymer is subjected to a combination of high shear and thermal gradients as it flows through the injection screw, runner system, and cavity, which strongly influences chain orientation, microstructural evolution, and final material performance. Inherent heterogeneities and the presence of fillers or degraded chains can further affect the structural evolution and mechanical properties of the molded parts [26]. Understanding and controlling the interplay between these heterogeneities, filler content, and processing conditions is therefore crucial to optimize injection molding of recycled materials, enabling the production of components that maintain structural integrity and functional performance despite the variability inherent to postconsumer or postindustrial polymer streams.

In the case of injection molding, the low viscosity of the molten polymer does not pose a processing limitation, as it facilitates easy filling of the mold and reduces the required injection pressure. For this reason, materials with a low viscosity profile, such as rM1, were selected and subjected to comprehensive mechanical characterization to assess their suitability for molding recycled components. Should specific processing requirements demand a higher melt viscosity, the formulation can be adjusted by blending rM1 with other materials, such as rM2, which exhibits higher viscosity and melt strength. For this purpose, blends of rM1 and rM2 were prepared at different ratios (90:10, 50:50, and 10:90). This approach not only allows tuning of the rheological properties to match the needs of particular injection molding operations but also enables anticipation of the effects of potential contamination, for example, by accidental mixing of M1 and M2 streams or in controlled 50:50 blends. By carefully

managing these combinations, it is possible to optimize flow behavior, maintain structural integrity, and achieve reproducible mechanical performance in molded parts, even when working with recycled polymer fractions with varying composition and inherent heterogeneities.

Tensile testing was performed on pure and blended formulations, where 100rM1 represents the formulation made entirely of rM1, 100rM2 is composed solely of rM2, and the other samples correspond to mixtures of rM1 and rM2 at the indicated ratios (90rM1_10rM2, 50rM1_50rM2, 10rM1_90rM2). Figure 4 reports representative images of the tested specimens together with a significant tensile curve, illustrating the mechanical response of the investigated formulations; a summary of the data is reported in Table S2.

100rM1 exhibits a tensile modulus of 1333 ± 26 MPa, a maximum tensile stress of 27.9 ± 0.8 MPa, and elongation at break of 4.4% ± 0.4%. In comparison, 100rM2 shows a tensile modulus of 1214 ± 26 MPa (−9% vs. 100rM1), tensile stress of 23.1 ± 0.3 MPa (−17%), and elongation at break of 4.1% ± 0.3%, reflecting its higher viscosity and filament-rich microstructure.

The blends of rM1 and rM2 do not strictly follow a linear interpolation between the pure materials. The 90rM1_10rM2 blend shows a tensile modulus of 1283 ± 2 MPa (−3.8% vs. 100rM1), tensile stress of 28.4 ± 0.3 MPa (slightly above 100rM1), and elongation at break of 5.4% ± 0.2% (+22%), indicating enhanced ductility. In the 50rM1_50rM2 blend, the tensile stress (24.6 ± 1.7 MPa, −12% vs. 100rM1) is lower than the linear average of the two pure materials, suggesting non-linear interactions between the homogeneous rM1 matrix and rM2 filaments. The 10rM1_90rM2 blend shows a tensile modulus of 1281 ± 34 MPa and tensile stress of 24.2 ± 0.3 MPa, slightly higher than expected from linear mixing, while elongation at break remains comparable to 100rM1 within the measurement uncertainty.

These results demonstrate that blending rM1 and rM2 allows controlled tuning of mechanical properties, but non-linear effects are observed due to microstructural interactions. This highlights the importance of experimental characterization when designing recycled or upcycled polymer blends for injection molding.

An important aspect for recycled polypropylene materials is the stability of mechanical properties upon blending. In the present study, tensile modulus, tensile stress, and elongation at break of rM1/rM2 blends varied by less than ~20% across all compositions, indicating that mixing does not significantly compromise performance. This suggests that these formulations can be effectively recycled without major loss of mechanical functionality.

This behavior is consistent with literature data for recycled PP (r-PP). In fact, studies on r-PP report tensile modulus values in the range of ~295–1200 MPa, tensile strengths above 20 MPa, and elongations at break typically ranging from 10% to 20%, depending on material source, degree of contamination, and processing conditions [33–35].

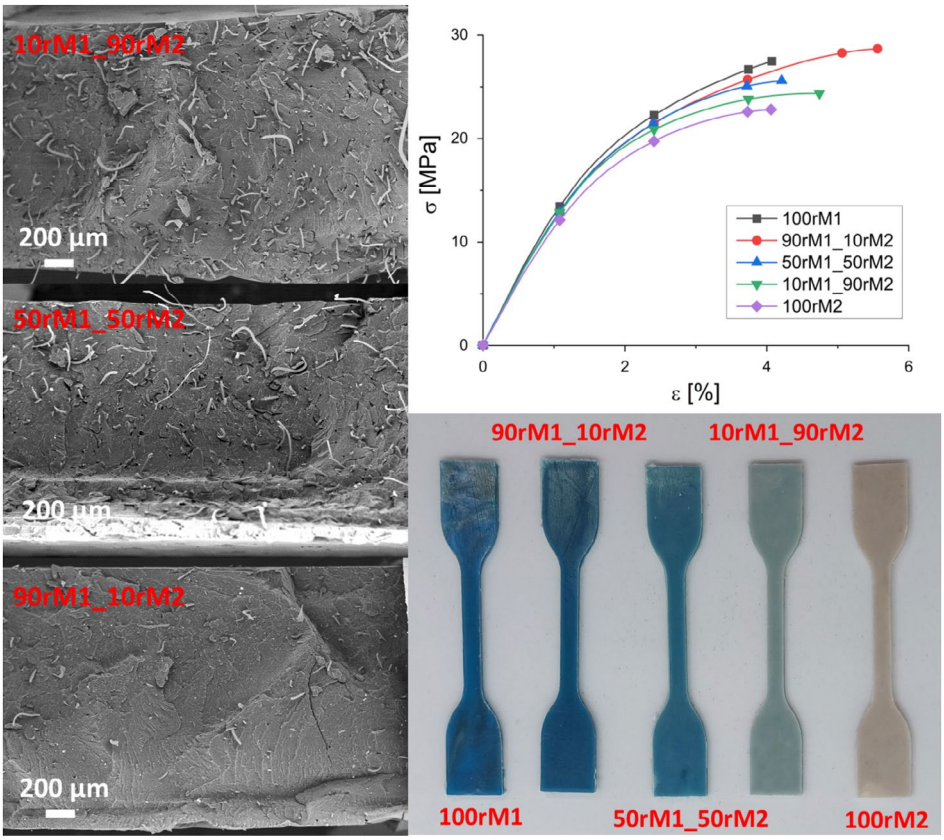

FIGURE 4 | SEM of the sections of injection molded parts recycled from masks coded rM1 and rM2; one stress–strain representative curve for each formulation and the visual aspect of the specimens.

SEM images of the fracture surfaces of the dog-bone specimens corresponding to the rM1/rM2 blends show a progressive increase in filament-like structures and voids associated with filament pull-out as the rM2 content increases. Such features are widely reported in polymer-based systems and composites, where interfacial debonding and pull-out mechanisms contribute to energy dissipation during tensile deformation and can delay final fracture. This behavior is consistent with the variations in elongation at break observed for the blended formulations, particularly at low rM2 contents, and agrees with failure mechanisms described in the literature for filament- or fiber-containing polypropylene systems [36].

3.3.2 | Film Extrusion

Film extrusion by flat-die extrusion followed by calendering requires a polymer melt with sufficient viscosity and stable shear-thinning behavior to ensure uniform flow, surface quality, and thickness control. Furthermore, the material should exhibit adequate behavior under non-isothermal elongational flow. For recycled polypropylene systems, these requirements are strongly influenced by material heterogeneity and possible degradation effects.

Based on the rheological results, rM3 was selected for film extrusion by calendering, as it combines a relatively high zero-shear viscosity (η_0) with a stable shear-thinning response, ensuring adequate melt resistance while maintaining good processability and adequate melt deformability. While rM2 could also be suitable in terms of melt strength, its internal filaments and associated heterogeneities made it less appropriate for producing defect-free calendered films. This selection highlights the importance of balancing rheological performance with material homogeneity for upcycled PP film applications.

Figure 5 shows the visual aspect of the rM3 cast film, highlighting a smooth and uniform surface. Samples were cut along the machine direction (MD) and transverse direction (TD) and subjected to tensile testing. The results (Table S3) reveal pronounced anisotropy: compared to MD, the TD exhibits a ~20% lower tensile modulus and a slightly lower tensile stress at yield, while the elongation at break increases almost fourfold, reflecting the higher ductility along the transverse direction.

SEM images of the tested film sections (rM3_section_MD and rM3_section_TD) provide further insight: the MD section is largely flat, without evident morphological features, whereas the TD section shows tapering structures parallel to the surface, resembling horizontal channels. These features likely result from the combination of flow-induced chain orientation during calendering and plastic deformation during tensile testing, and they may facilitate the higher ductility observed in the TD. Similar behaviour has been reported in cast and calendered polypropylene films, where chain orientation and deformation during testing contribute to anisotropic mechanical properties, even when the MD shows minimal visible microstructural evidence [37].

3.3.3 | 3D Printing

The selection of materials for 3D printing was guided primarily by their rheological properties measured in oscillatory shear and their suitability for extrusion-based additive manufacturing. rM2 exhibited a high zero-shear viscosity and a pronounced yield stress, features that favor shape retention and filament stability during printing [29]. However, using rM2 alone proved challenging, as its high viscosity and yield stress made extrusion less consistent. The measured filament diameter was always slightly lower than the nominal value, although the roundness was fairly preserved, as shown in Figure S10 and Table S4.

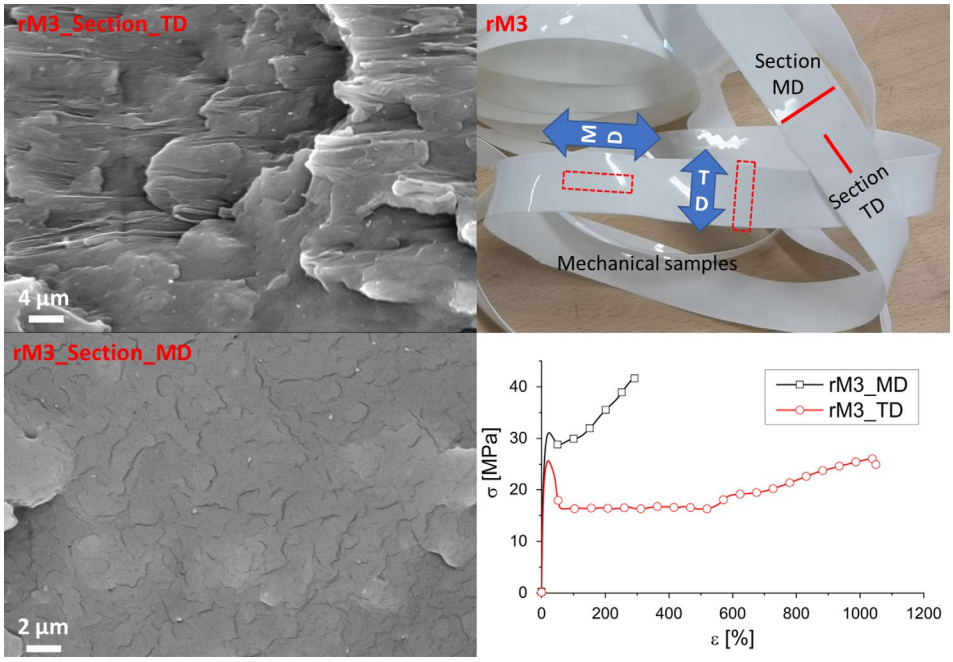

FIGURE 5 | Visual aspect of the film obtained by casting (rM3) and identification of samples for analysis in machine direction (MD) and transverse direction (TD); SEM of the sections of cast film and one stress–strain representative curve for each direction.

To overcome this issue, blends with rM1 were prepared on a small scale using a mini-extruder, allowing modulation of flow properties and facilitating filament formation.

The blends investigated included 10rM1_90rM2, 30rM1_70rM2, and 50rM1_50rM2, while rM2 alone served as a reference. Rheological data fitted with the modified Carreau model (data in Table 3 and Figure 6) show that increasing rM2 content results in higher viscosity, longer relaxation times, and more pronounced shear thinning behaviour, affecting the extrusion behaviour of the blends.

DSC analyses (data in Table S5 and Figure 6) indicate that the melting temperatures of PE, PP, and PET remain essentially constant across all rM2-rich blends. The melting enthalpy of PE increases with higher rM2 content, while PP enthalpy decreases modestly, and PET contributions are small but detectable. The total enthalpy (ΔH_m, Tot) remains relatively constant, suggesting stable crystallinity across the blends. This stability is important for 3D printing because it ensures predictable solidification and minimizes warpage and interlayer defects [38].

Figure 7 presents SEM images of the external surface of the filaments, the cross-section of the filaments, and a cross-section of a 3D printed nut with six faces, showing representative formulations 100rM2, 10rM1_90rM2, and 50rM1_50rM2. The filament surfaces appear rough in all cases, due to the use of recycled material containing residual fibers, partially infused within the matrix. In the cross-sections, the 50rM1_50rM2 blend shows greater deviation from a circular shape, reflecting anisotropy in solidification during filament formation, which can inevitably lead to challenges during 3D printing. Filament diameter stability was quantitatively assessed by measuring two orthogonal diameters (D1 and D2 in Figure S10 and Table S4) along the filament and calculating their deviation. The results reveal a non-negligible degree of ovalization, indicating deviations from ideal circular cross-sections (1.75 mm), which depend on composition. Notably, increasing rM2 content results in enhanced dimensional stability and reduced ovality.

Observations of the printed nuts reveal that 100rM2 exhibits stringing connecting the different infill portions of the component, 10rM1_90rM2 shows a more faithful replication with only minor stringing, and 50rM1_50rM2 again displays more pronounced stringing. These features are consistent with literature reports on recycled polypropylene blends, where residual fibers and anisotropic solidification can influence filament morphology, surface roughness, and interlayer adhesion, emphasizing the need for careful rheological control to minimize printing defects [38].

TABLE 3 | Modified Carreau model parameters used for fitting the rheological curves of rM1-rM2 blends obtained at 230°C.

	η_0 [Pa×s]	λ [1/s]	n	σ_0 [Pa]	R^2
50rM1_50rM2	509	0.99	0.73	66.3	0.99
30rM1_70rM2	694	1.06	0.69	187	0.99
10rM1_90rM2	748	1.15	0.66	276	0.99
100rM2	774	0.84	0.61	332	0.99

4 | Conclusions

This work demonstrates that postuse masks can be effectively recycled and upcycled into materials suitable for multiple polymer processing techniques. Surgical and FFP2 masks were carefully characterized, revealing that PP and PE are the predominant components, while minor fractions of PET and cellulose fibers are also present. ATR-FTIR and SEM–EDX analyses confirmed the presence of inorganic fillers ($CaCO_3$) in rM1 and embedded polymeric fibers in rM2, whereas rM3 showed a homogeneous polymeric matrix.

Rheological characterization revealed that the materials exhibit distinct behaviors depending on microstructure. rM1 has the lowest viscosity and negligible yield stress, suitable for injection molding, where low melt viscosity facilitates mold filling and minimizes pressure requirements. rM2 displays higher zero-shear viscosity, pronounced shear-thinning, and significant yield stress, making it more appropriate for 3D printing, as it supports filament stability, shape retention, and dimensional fidelity. rM3, with intermediate viscosity and stable shear-thinning, is suitable for film extrusion via calendering, producing films with uniform surfaces and anisotropic mechanical behavior due to chain orientation in machine and transverse directions.

Blending strategies using rM1 and rM2 allowed fine-tuning of rheological properties.

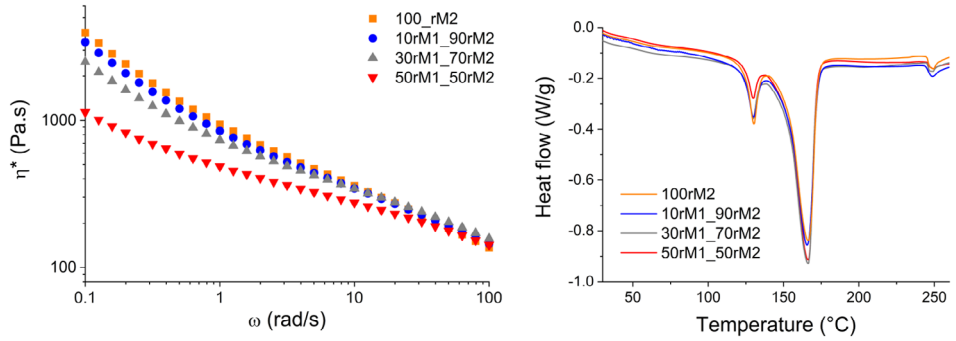

FIGURE 6 | Rheological experimental point obtained at 230°C and DSC characteristic plots for rM2-rM1 blends obtained from small scale blending.

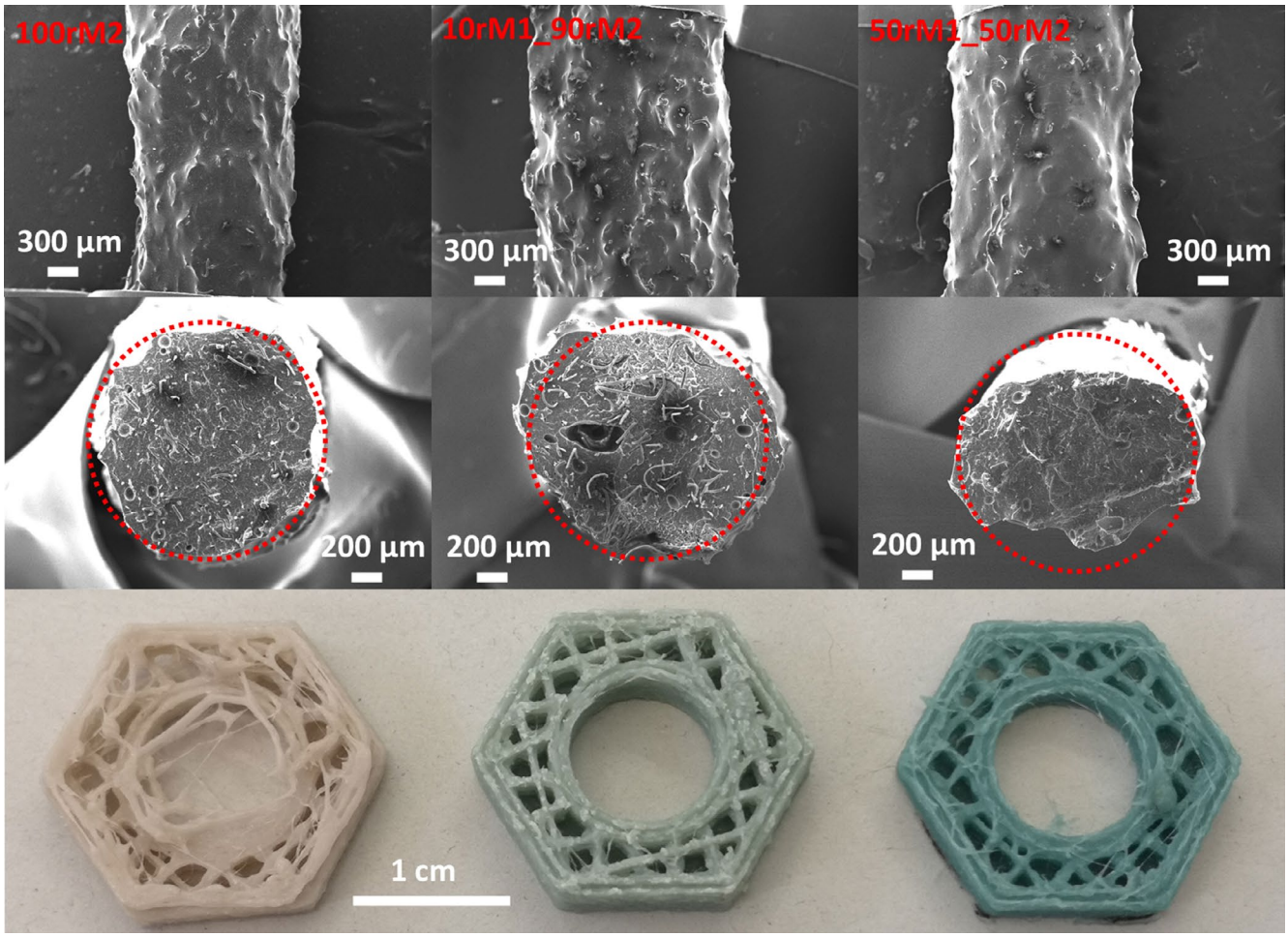

FIGURE 7 | SEM images of the surface and section of filaments used for material extrusion additive manufacturing technique and sections of 3D printed parts.

Mechanical testing of injection-molded specimens showed that blending rM1 and rM2 allows controlled tuning of properties, with tensile modulus, stress, and elongation varying by less than ~20%, demonstrating that mechanical performance is largely preserved despite material heterogeneity. The morphological features are correlated with mechanical responses, where filament pull-out and interfacial debonding contributed to energy dissipation and elongation at break.

DSC analyses confirmed that overall melting temperatures and total enthalpy remain largely unchanged across rM2-rich blends, ensuring stable crystallinity critical for extrusion-based additive manufacturing. SEM observations of filaments revealed surface roughness, deviations from circular cross-sections, and stringing effects, particularly in blends with intermediate compositions (50rM1_50rM2), consistent with the presence of residual fibers and anisotropic solidification.

Similarly, film extrusion with rM3 produced defect-free, smooth cast films with predictable anisotropic mechanical behaviour.

Overall, this study confirms that recycled mask materials can be valorized into functional polymer feedstocks for different processing technologies. By selecting materials based on rheological behavior and microstructural features, it is possible to optimize injection molding, 3D printing, and film extrusion, producing components with reliable mechanical performance and processing stability. These findings demonstrate the feasibility of upcycling postconsumer masks, providing a sustainable route for polymer reuse while maintaining processability and end-use functionality.

Author Contributions

Daniele Battegazzore: conceptualization, writing – review and editing, writing – original draft, visualization, validation, data curation. **Fulvia Cravero:** investigation, formal analysis, visualization, writing – original draft, data curation. **Giulia Bernagozzi:** data curation, formal analysis, visualization, investigation, writing – original draft. **Rossella Arrigo:** investigation, validation, writing – review and editing, data curation, methodology. **Alberto Frache:** conceptualization, writing – review and editing, supervision, methodology.

Acknowledgments

The authors would like to thank Mrs. Giuseppina Iacono for SEM analysis, Mr. Giovanni Balladore and Mr. Paolo Bolognesi for the work during their master thesis and the support of the Mondovì municipality and Circolo delle Idee for the after use mask supply. During the preparation of this work the author(s) used Chat GPT in order to improve grammar, readability, and overall language quality. After using this tool/service,

the author(s) reviewed and edited the content as needed and take(s) full responsibility for the content of the published article. Open access publishing facilitated by Politecnico di Torino, as part of the Wiley - CRUI-CARE agreement.

Funding

The authors have nothing to report.

Conflicts of Interest

The authors declare no conflicts of interest.

Data Availability Statement

The data that support the findings of this study are available from the corresponding author upon reasonable request.

References

1. IndexBox, "Nonwoven Fabric: World Market Overview 2024," 2025, IndexBox.

2. OECD, *Global Plastics Outlook: Economic Drivers, Environmental Impacts and Policy Options* (OECD Publishing, 2022).

3. O.W.i, "Data, Packaging Is the Source of 40 Percent of the Planet's Plastic Waste," 2024, https://ourworldindata.org.

4. Eurostat, *Packaging Waste Statistics – 2023 Data* (European Commission, 2025).

5. W.H. Organization, *Advice on the Use of Masks in the Context of COVID-19* (World Health Organization, 2020).

6. K. P. Roberts, S. C. Phang, J. B. Williams, et al., "Increased Personal Protective Equipment Litter as a Result of COVID-19 Measures," *Nature Sustainability* 5, no. 3 (2021): 272–279.

7. J. J. Klemes, Y. V. Fan, and P. Jiang, "The Energy and Environmental Footprints of COVID-19 Fighting Measures - PPE, Disinfection, Supply Chains," *Energy* 211 (2020): 118701.

8. I. Armentano, M. Barbanera, E. Carota, et al., "Polymer Materials for Respiratory Protection: Processing," *End Use, and Testing Methods, ACS Applied Polymer Materials* 3, no. 2 (2021): 531–548.

9. I.S. Ore, "Il Paradosso Delle Mascherine Fuori Norma: Lo Stato Paga Più di un Milione di Euro al Mese. Il Sole 24 Ore; 2024, 2023," 2026, https://www.ilsole24ore.com/art/il-paradosso-mascherine-fuori-norma-stato-paga-piu-un-milione-euro-mese-AEHwwJKB.

10. G.V. Research, *Surgical Masks Market (2023–2030)* (Grand View Research, 2024).

11. D. Battegazzore, F. Cravero, and A. Frache, "Is It Possible to Mechanical Recycle the Materials of the Disposable Filtering Masks?," *Polymers (Basel)* 12, no. 11 (2020): 2726.

12. S. Pourebrahimi, "Upcycling Face Mask Wastes Generated During COVID-19 Into Value-Added Engineering Materials: A Review," *Science of the Total Environment* 851, no. Pt 2 (2022): 158396.

13. C. Crespo, G. Ibarz, C. Saenz, P. Gonzalez, and S. Roche, "Study of Recycling Potential of FFP2 Face Masks and Characterization of the Plastic Mix-Material Obtained. A Way of Reducing Waste in Times of Covid-19," *Waste Biomass Valorization* 12 (2021): 1–10.

14. M. H. Chua, W. Cheng, S. S. Goh, et al., "Face Masks in the New COVID-19 Normal: Materials, Testing, and Perspectives," *Research (Wash D C)* 2020 (2020): 7286735.

15. K. O'Dowd, K. M. Nair, P. Forouzandeh, et al., "Face Masks and Respirators in the Fight Against the COVID-19 Pandemic: A Review of Current Materials, Advances and Future Perspectives," *Materials (Basel)* 13, no. 15 (2020): 3363.

16. X. Zhao, B. Boruah, K. F. Chin, M. Dokic, J. M. Modak, and H. S. Soo, "Upcycling to Sustainably Reuse Plastics," *Advanced Materials* 34, no. 25 (2022): e2100843.

17. Z. O. G. Schyns and M. P. Shaver, "Mechanical Recycling of Packaging Plastics: A Review," *Macromolecular Rapid Communications* 42, no. 3 (2021): e2000415.

18. O. Zabihi, R. Patrick, M. Ahmadi, et al., "Mechanical Upcycling of Single-Use Face Mask Waste Into High-Performance Composites: An Ecofriendly Approach With Cost-Benefit Analysis," *Science of the Total Environment* 919 (2024): 170469.

19. G. Infurna, A. Romani, M. C. Riccelli, M. Levi, L. Incarnato, and N. T. Dintcheva, "Recycling of Personal Protective Equipment: Sanitisation, Degradation and Polymer Blend Formulations," *Polymer Degradation and Stability* 234 (2025): 111249.

20. E. C. Emenike, K. O. Iwuozor, S. A. Agbana, K. S. Otoikhian, and A. G. Adeniyi, "Efficient Recycling of Disposable Face Masks via Co-Carbonization With Waste Biomass: A Pathway to a Cleaner Environment," *Cleaner Environmental Systems* 6 (2022): 100094.

21. D. Battegazzore, F. Cravero, and A. Frache, "Development of Disposable Filtering Mask Recycled Materials: Impact of Blending With Recycled Mixed Polyolefin and Their Aging Stability," *Resources, Conservation and Recycling* 177 (2022): 105974.

22. W. Ahmed and C. W. Lim, "Effective Recycling of Disposable Medical Face Masks for Sustainable Green Concrete via a New Fiber Hybridization Technique," *Construction and Building Materials* 344 (2022): 128245.

23. D. Battegazzore, F. Cravero, G. Bernagozzi, and A. Frache, "Designing a 3D Printable Polypropylene-Based Material From After Use Recycled Disposable Masks," *Materials Today Communications* 32 (2022): 103997.

24. M. Gahleitner, "Melt Rheology of Polyolefins," *Progress in Polymer Science* 26, no. 6 (2001): 895–944.

25. L. Sangroniz, M. Fernández, and A. Santamaria, "Polymers and Rheology: A Tale of Give and Take," *Polymer* 271 (2023): 125811.

26. F. Cravero, R. Arrigo, and A. Frache, "Processing-Driven Structuring of Polymer-Based Materials: A Brief Overview," *Polymers (Basel)* 17, no. 18 (2025): 2483.

27. R. Arrigo and A. Frache, "FDM Printability of PLA Based-Materials: The Key Role of the Rheological Behavior," *Polymers (Basel)* 14, no. 9 (2022): 1754.

28. R. Maderuelo-Sanz, P. Acedo-Fuentes, F. J. Garcia-Cobos, F. J. Sanchez-Delgado, M. I. Mota-Lopez, and J. M. Meneses-Rodriguez, "The Recycling of Surgical Face Masks as Sound Porous Absorbers: Preliminary Evaluation," *Science of the Total Environment* 786 (2021): 147461.

29. R. Arrigo, D. Battegazzore, G. Bernagozzi, F. Cravero, D. N. R. Pedraza, and A. Frache, "Recycled PP for 3D Printing: Material and Processing Optimization Through Design of Experiment," *Applied Sciences-Basel* 12, no. 21 (2022): 10840.

30. R. Arrigo, G. Malucelli, and F. P. Mantia, "Effect of the Elongational Flow on the Morphology and Properties of Polymer Systems: A Brief Review," *Polymers (Basel)* 13, no. 20 (2021): 3529.

31. L. Sangroniz, M. Fernandez, P. Partal, and A. Santamaria, "Rheology of Polymer Processing in Spain (1995-2020)," *Polymers (Basel)* 13, no. 14 (2021): 2314.

32. R. Banerjee and S. S. Ray, "Role of Rheology in Morphology Development and Advanced Processing of Thermoplastic Polymer Materials: A Review," *ACS Omega* 8, no. 31 (2023): 27969–28001.

33. T. Jamnongkan, N. Intraramongkol, W. Samoechip, et al., "Towards a Circular Economy: Study of the Mechanical, Thermal, and Electrical Properties of Recycled Polypropylene and Their Composite Materials," *Polymers (Basel)* 14, no. 24 (2022): 5482.

34. S. U. Handayani, M. Fahrudin, W. Mangestiyono, and A. F. Hadi Muhamad, "Mechanical Properties of Commercial Recycled Polypropylene From Plastic Waste," *Journal of Vocational Studies on Applied Research* 3, no. 1 (2021): 1–4.

35. T. Zhiltsova and M. S. A. Oliveira, "Sustainable Polypropylene Blends: Balancing Recycled Content With Processability and Performance," *Polymers (Basel)* 17, no. 11 (2025): 1556.

36. S. Y. Fu, B. Lauke, E. Mäder, C. Y. Yue, and X. Hu, "Tensile Properties of Short-Glass-Fiber- and Short-Carbon-Fiber-Reinforced Polypropylene Composites," *Composites Part A: Applied Science and Manufacturing* 31, no. 10 (2000): 1117–1125.

37. S. H. Tabatabaei, P. J. Carreau, and A. Ajji, "Effect of Processing on the Crystalline Orientation, Morphology, and Mechanical Properties of Polypropylene Cast Films and Microporous Membrane Formation," *Polymer* 50, no. 17 (2009): 4228–4240.

38. M. Bertolino, D. Battegazzore, R. Arrigo, and A. Frache, "Designing 3D Printable Polypropylene: Material and Process Optimisation Through Rheology," *Additive Manufacturing* 40 (2021): 101944.

Supporting Information

Additional supporting information can be found online in the Supporting Information section. **Figure S1:** LEISTRITZ ZSE 18/40 D screw profile (a) and flat die for casting (b). **Figure S2:** Felfil Evo filament making machine scheme. **Figure S3:** RheoSpin apparatus: a series of pulley (1, 2, 3) grab the filament coming out from the extruder and delivers it to a traction pulley (4) rotating at steady speed or steady acceleration. Pulley 5 prevents slipping of the filament from pulley 4. The load cell (connected to pulley 2) measures the force on the filament in a range between 0.1–100 cN with a sensitivity of 0.1 cN. At the breaking of the filament, the current force and speed are registered. **Figure S4:** FTIR-ATR characterization of M3 surgical face mask. **Figure S5:** Statistical report of the 18 types of FFP2 collected and used for the M2 material. **Figure S6:** FTIR-ATR characterization of type E FFP2 masks. **Figure S7:** FTIR-ATR characterization of type S FFP2 masks. **Figure S8:** FTIR-ATR characterization of type B FFP2 masks. **Figure S9:** DSC analyses of rM2. **Table S1:** RheoSpin data of rM1 and rM3 materials. **Table S2:** Mechanical properties of injection molded specimens (tensile modulus (E), maximum tensile stress (σ) and deformation at break (ε)) of the rM1-rM2 system. **Table S3:** Mechanical properties of cast film specimens (tensile modulus (E), tensile stress at yield (σ_y) and deformation at break (ε)) of the rM3 material. **Figure S10:** SEM images with D1 and D2 measurements of 100rM2, 10rM1_90rM2, 50rM1_50rM2. **Table S4:** Dimensional measurement analysis from SEM images. **Table S5:** Characteristic data obtained from DSC analyses.